PHYSICAL REVIEW VOLUME 179, NUMBER 4 20 MARCH 1969

Effect of Nuclear Polarization on the Giant Dipole Resonance of Ho^{165}†

M. A. KELLY,* B. L. BERMAN, R. L. BRAMBLETT,‡ AND S. C. FULTZ
Lawrence Radiation Laboratory, University of California, Livermore, California 94550

(Received 25 November 1968)

The (γ, n) and $(\gamma, 2n)$ cross sections of polarized Ho^{165} were measured between 10 and 21 MeV using the nearly monoenergetic photon beam from the annihilation in flight of fast positrons. Two independent cross sections were obtained by orienting the polarization axis of the target nuclei perpendicular to and parallel to the photon beam. From these, the cross sections corresponding to the intrinsic modes of the giant resonance were computed. The target consisted of nine single crystals of holmium metal having a total mass of 50 g, and was polarized by cooling to approximately 0.13°K in the presence of a 15-kOe magnetic field. The alignment parameter f_2 was determined to be 0.43 ± 0.05 by measuring the anisotropy of the γ rays emitted by Ho^{166m} (created in the target by neutron activation). Both major peaks of the total photoneutron cross section, $\sigma_t=\sigma[(\gamma, n)+(\gamma, pn)+(\gamma, 2n)]$, exhibited a dependence upon target orientation that agrees qualitatively with the collective model for deformed nuclei. The observed anisotropy was $(74\pm13)\%$ of that predicted by hydrodynamic models.

I. INTRODUCTION

DURING the last two decades, numerous studies have shown that the photonuclear giant dipole resonance is closely related to the gross properties of nuclei. Its mean energy and width, for example, are relatively insensitive to variations of the nuclear level density or to individual nucleon effects in nuclei with atomic number $A>50$,[1] yet are strongly correlated to the nuclear size and deformation. This experiment is concerned with the nuclear shape-dependent aspects of the giant resonance. Both collective models[2-4] and the independent particle model[5] predict that the giant resonance of a deformed nucleus is split as a result of its nonspherical nuclear potential, and as a consequence its photon absorption cross section is a function of nuclear orientation. According to these models, one can measure the anisotropy (i.e., the change in this cross section as a function of the angle between the nuclear symmetry axis and an incident photon beam) by observing the photon absorption of a polarized target, since in this case one can excite preferentially the giant resonance components related to specific intrinsic coordinates of the nucleus. For heavy nuclei, the photon absorption can be determined quite conveniently by measuring their total photoneutron cross section, since the competing channels for deexcitation, namely, proton emission and electromagnetic decay, are much less favored. An experiment showing that this "anisotropy" does exist in Ho^{165} was reported by Ambler *et al.*[6] The present experiment expands on this earlier measurement by providing the detailed energy dependence of the anisotropy. It consists of obtaining the total photoneutron cross section $\sigma_t=\sigma[(\gamma, n)+(\gamma, pn)+(\gamma, 2n)]$ of a polarized Ho^{165} target in the giant resonance region (10–20 MeV), from measurements of the partial cross sections $\sigma(\gamma, n)$ and $\sigma(\gamma, 2n)$. The experiment had two main objectives: (1) to measure the separate cross sections of the shape-dependent components of the giant resonance, and (2) to check the detailed predictions of two collective models.

II. THEORY

A. Collective Model of the Giant Dipole Resonance

The collective hydrodynamic model has been quite successful in explaining many properties of the giant dipole resonance in the photoabsorption cross section of heavy nuclei. This model pictures the nucleus as two interpenetrating fluids which represent the proton and neutron densities in the nuclear matter, and which can be displaced with respect to each other by an appropriate excitation. Though very simple conceptually, it explains reasonably well the variation of the giant resonance energy with mass number A, and the distribution of dipole strengths measured experimentally.

The first application of this model to the nuclear photoeffect was made by Goldhaber and Teller[7] in 1948. Considering the two fluids to be incompressible and of uniform density, they calculated the classical energy of the dipole vibration that results from a linear displacement of the two fluids in a spherical nucleus.

A variation of this elementary model, also suggested by Goldhaber and Teller but developed in detail by Steinwedel and Jensen,[8] assumes that the total nuclear density, i.e., the sum of the neutron and proton densities, is constant at every point in the nucleus, but that the local density of the protons can vary relative to the neutron density. For the dipole vibration energy,

---

† Work performed under the auspices of the U.S. Atomic Energy Commission.

* Present address: Hewlett Packard Corp., Palo Alto, Calif.

‡ Present address: General Atomics Atomic, San Diego, Calif.

[1] B. L. Berman, J. T. Caldwell, R. R. Harvey, M. A. Kelly, R. L. Bramblett, and S. C. Fultz, Phys. Rev. **162**, 1098 (1967).

[2] K. Okamoto, Phys. Rev. **110**, 143 (1958).

[3] M. Danos, Nucl. Phys. **5**, 23 (1958).

[4] M. Danos and W. Greiner, Phys. Rev. **134**, B284 (1964).

[5] D. H. Wilkinson, Phil. Mag. **3**, 567 (1958).

[6] E. Ambler, E. G. Fuller, and H. Marshak, Phys. Rev. **138**, B117 (1965).

[7] M. Goldhaber and E. Teller, Phys. Rev. **74**, 1046 (1948).

[8] H. Steinwedel and H. Jensen, Z. Naturforsch. **5a**, 413 (1950).

they obtain

$$E=(4ZN/A^2)(12.5/A^{1/3})K^{1/2}\ (E \text{ in MeV}), \qquad (1)$$

where K is the symmetry energy constant from the semiempirical mass formula, in MeV, and Z, N, and A are the atomic, neutron, and mass numbers, respectively. Both of these elementary models predict a variation of the giant resonance energy with A which agrees rather well with experimental values. Inherent in both models is the assumption that all the nucleons participate in the dipole vibration, and hence the absorption cross section calculated for the giant resonance exhausts the dipole sum-rule value.

The latter model has been generalized for the case of deformed nuclei by Okamoto[2] and independently by Danos.[3] They showed that since these nuclei are spheroidal, the energies of the normal modes of the dipole vibration are no longer degenerate, but instead, depend on the lengths of the principal axes of the spheroid. Hence, one obtains a different energy for displacements of the two fluids along the nuclear quantization axis then for displacements along the two transverse axes. Relating this "splitting" of the giant resonance to nuclear deformation, Danos[3] obtains

$$E_b/E_a=0.911(a/b)+0.089, \qquad (2)$$

where E_b is the energy of two degenerate vibrations perpendicular to the nuclear symmetry axis, E_a is the energy of the vibration along the symmetry axis, and a and b are the semimajor and semiminor axes of the nucleus, respectively. These axes are related to the intrinsic electric quadrupole moment Q_0 by the relation $Q_0=\frac{2}{5}Z(a^2-b^2)$. This splitting of the giant resonance is seen experimentally in highly deformed nuclei, such as Ho^{165}.[9,10] Even in slightly deformed nuclei where the resonance shows only a single peak, Okamoto has shown that the over-all width of the resonance is strongly correlated to the nuclear deformation as measured by the intrinsic quadrupole moment.

A more sophisticated collective model, but one that still retains the two-fluid mechanism, is the dynamic model of Danos and Greiner.[4] They include the effect of coupling between the fluid oscillations and the surface rotational and vibrational degrees of freedom. Qualitatively, this model predicts that these surface modes enrich the spectrum in the giant resonance region considerably and that for high deformations their effect is to remove the degeneracy of the vibrational modes perpendicular to the intrinsic axis, so that the time-averaged shape of the nucleus is "triaxial." Detailed calculations of the the photoabsorption cross section of Ho^{165} have been made using this model; these are outlined in Sec. III.

The simplicity of these collective models makes them quite useful for obtaining quantitative relations between the model parameters and experimental data, and perhaps of more importance, they work well despite their simplicity. There are, however, fundamental limitations to these models, primarily because they neglect completely individual particle motions. Thus it is difficult to provide a rigorous quantum-mechanical mechanism for the dipole vibrations based on what is known of the strong interaction, or to incorporate into the model a mechanism by which these vibrations deexcite, thereby explaining their width.

The independent particle model, on the other hand, potentially can solve these and other problems, but unfortunately, detailed calculations have been made only for lighter nuclei. Wilkinson[5] has pointed out that this model predicts a clustering of levels having a spin and parity of 1^- with respect to the ground state, and if one uses an effective nucleon mass of approximately $0.5\ M_n$, where M_n is the nucleon mass, the energy of the cluster corresponds to that of the giant resonance. For highly deformed nuclei, one sees a splitting of the giant resonance as in the collective model. Because of the lack of quantitative calculations for heavier nuclei, however, a detailed comparison with the present experiment as yet cannot be made.

B. Photon Absorption Cross Section of Oriented Deformed Nuclei

Using the optical theorem, the photon absorption cross section σ_a of oriented nuclei can be written

$$\sigma_a=(4\pi/k)\ \mathrm{Im}\sum_m a_m R_{mm}, \qquad (3)$$

where k is the photon momentum, a_m is the magnetic substate population normalized so that $\sum_m a_m=1$, and R_{mm} is the forward elastic scattering amplitude.

The forward scattering amplitude has been evaluated[6] for a nucleus in which the rotational and intrinsic wave functions are separable, and in a more general form by Arenhövel *et al.*[11] These authors express the scattering amplitude in terms of intrinsic matrix elements, which they evaluate using the dynamic collective model.

The former authors obtain an expression for the cross section in the form

$$\sigma_a=\sum_\nu f_\nu(T)\sigma_\nu(E)P_\nu(\cos\theta), \qquad (4)$$

which shows the explicit dependence of the cross section on the degree of nuclear orientation expressed in terms of the parameters $f_\nu(T)$ of Tolhoek and Cox,[12] which form a representation of the magnetic substate population in spherical harmonics. Specifically, $f_1(T)$ is

---

[9] E. G. Fuller and E. Hayward, Nucl. Phys. **30**, 613 (1962).

[10] R. L. Bramblett, J. T. Caldwell, G. F. Auchampaugh, and S. C. Fultz, Phys. Rev. **129**, 2723 (1963).

[11] H. Arenhövel, M. Danos, and W. Greiner, Phys. Rev. **157**, 1109 (1967).

[12] H. A. Tolhoek and J. A. M. Cox, Physica **19**, 109 (1953).

defined by

$$f_1(T)=(1/I)\sum_m ma_m, \tag{5a}$$

where I is the nuclear spin and m is the magnetic quantum number. The term $f_1(T)$ is referred to as the polarization parameter, and

$$f_2(T)=(1/I^2)\left[\sum_m m^2a_m-\tfrac{1}{3}I(I+1)\right] \tag{5b}$$

is the alignment parameter. The dependence of the cross section upon the orientation of the target is specified explicitly through the Legendre polynomials $P_\nu(\cos\theta)$, where θ is the angle between the incident photon beam and the target quantization axis. Symmetry conditions require that for an unpolarized photon beam only even values of ν enter, and that if only electric dipole excitations are considered, $\nu=0$ or 2. For dipole excitations,

$$\begin{aligned}\sigma_\nu=4\pi k\binom{2\nu}{\nu}I_i^\tau\left[\frac{(2I_i+1)(2I_i-\nu)!}{(2I_i+\nu+1)!}\right]^{1/2}\langle I_iK_i\nu0\mid I_iK_i\rangle\\ \times\langle 111-1\mid\nu0\rangle\sum_{\Delta K}(-)^{\Delta K+1}\langle 1\,\Delta K\,1\,-\Delta K\mid\nu0\rangle\\ \times\sum_n\mid\langle n\mid Q_1\mid i\rangle\mid^2\frac{EE_n\Gamma_n}{(E_n^2-E^2)^2+\Gamma_n^2E^2},\end{aligned} \tag{6}$$

where I_i is the spin of the ground state, and K_i its projection on the nuclear symmetry axis; K_n is the projection of the spin of state n on the nuclear symmetry axis; k is the wave number of the incident photon; $\langle n\mid Q_1\mid i\rangle$ is the electric-dipole matrix element where i and n are the intrinsic nuclear wave functions of the dynamic collective model for the ground state and giant dipole states, respectively; E_n and Γ_n are the mean energy and width of the nth resonances, respectively; E is the incident photon energy; and $\Delta K=K_i-K_n$.

The giant dipole states associated with the nuclear symmetry axis (parallel mode) are those for which $\Delta K=0$, while for those states associated with the perpendicular modes, $\Delta K=\pm1$. As one would expect from the qualitative picture of the giant resonance presented in Sec. I, those states for which $\Delta K=\pm1$ maintain their same relative strengths regardless of the degree of polarization in the target, as do those states for which $\Delta K=0$. Orienting the target changes only the strengths of these two groups with respect to each other. We can, therefore, define two intrinsic cross sections, $\sigma_{||}$ and $\sigma_\perp$, which refer respectively to excitation of modes parallel to and perpendicular to the nuclear symmetry axis,

$$\begin{aligned}\sigma_{||}=\delta_{\Delta K,0}\frac{4\pi k}{3}\sum_n\mid\langle n\mid Q_1\mid i\rangle\mid^2\frac{EE_n\Gamma_n}{(E_n^2-E^2)^2+E^2\Gamma_n^2},\\ \sigma_\perp=\delta_{\Delta K,\pm1}\frac{4\pi k}{3}\sum_n\mid\langle n\mid Q_1\mid i\rangle\mid^2\frac{EE_n\Gamma_n}{(E_n^2-E^2)^2+E^2\Gamma_n^2},\end{aligned} \tag{7}$$

where δ is the Kronecker delta function.

Evaluating Eq. (4) in terms of these cross sections and the appropriate ground-state parameters for Ho^{165} $(I_i=K_i=\frac{7}{2})$, we obtain

$$\begin{aligned}\sigma_a(E,\theta,T)=(\sigma_{||}+\sigma_\perp)\\ +0.4083(\sigma_\perp-2\sigma_{||})f_2(T)P_2(\cos\theta).\end{aligned} \tag{8}$$

Qualitatively, we see from this expression that if $\theta=0°$ (i.e., the target polarization axis is parallel to the incident photon beam), the dipole modes represented by $\sigma_\perp$ are enhanced by nuclear polarization, while those associated with $\sigma_{||}$ are diminished. Since the collective model correlates the lower-energy resonance with $\sigma_{||}$ and the higher-energy resonance with $\sigma_\perp$, the higher-energy resonance component should be enhanced and the lower one reduced, whereas for $\theta=90°$, the lower-energy resonance should be enhanced and the higher one should be diminished, but the effect should be only half as large as for the $\theta=0°$ case.

Using this expression and the dipole strengths calculated from the dynamic collective model and making some assumptions about the widths of the associated levels, one can make a quantitative calculation of the magnitude and energy dependence of the photon absorption cross section for an oriented holmium target. Alternately, since the model-dependent features of the calculations of Ref. 2 lie primarily in the nuclear matrix elements themselves, the relationship between the experimentally observed cross sections and the two intrinsic cross sections, $\sigma_{||}$ and $\sigma_\perp$, is nearly model-independent.[13] Consequently, one can calculate these intrinsic cross sections from the data. Both of these approaches have been followed in analyzing the experimental data.

III. DESCRIPTION OF THE EXPERIMENT

From the predictions of the collective model just discussed, the total photoneutron cross section σ_t of a completely polarized target of Ho^{165} should differ from the unpolarized cross section by at most 40% for the lower-energy resonance component and by 20% for the higher-energy component. Several factors incorporated into the present experiment made it possible to measure this difference with considerably better accuracy than was possible in any previous experiment, and to obtain the details of its dependence upon photon energy. These are outlined briefly below and are described in more detail later in this section.

The first of these factors is the large target mass. By using single crystals of holmium metal, a polarized target was constructed that contained approximately $\frac{1}{3}$ mole of holmium and a negligible amount of other materials. The neutrons produced in this relatively large target outnumbered those originating from background sources [(γ, n) reactions in the cryostat win-

---

[13] The assumptions needed to obtain Eq. (8) are (a) the nuclear wave function can be written as a product of an intrinsic part χ_n and a rotational part $D_{MK}{}^I$, and (b) the energy differences between different rotational levels are negligible, so that one can sum over states (see Ref. 6).

dows, cosmic background, etc.] by a factor of at least 20, so that the uncertainty in the measured cross sections arising from background corrections was small.

A second factor was the photon energy spectrum. By using the technique of obtaining nearly monoenergetic photons from the annihilation of fast positrons, no "unfolding" of the photon spectrum was necessary in order to obtain the net neutron yield for a given photon energy, as is necessary if bremsstrahlung photons are used. To obtain a cross section with the latter spectrum, the measured quantities (the total number of neutrons produced for a given peak photon energy) must be determined much more precisely than the resulting accuracy of the cross section. While the positrons yield a photon spectrum containing a bremsstrahlung component, this component contributes only a relatively small amount to the total number of neutrons produced in the target (20% at 12 MeV and 50% at 20 MeV) which can be measured accurately. Consequently, one can accurately correct for this contribution, and the resulting cross section has a statistical uncertainty only slightly greater than that for the total number of neutrons produced.

The third factor was the ability to determine the neutron multiplicity; i.e., the ability to distinguish neutrons produced by $(\gamma, 2n)$ events from those produced by (γ, n) events. This is quite important in determining the absolute cross section, since in most elements, $(\gamma, 2n)$ processes dominate at higher energies. Knowing the neutron multiplicity permits one to convert the measured neutron yield cross section $\sigma_y = \sigma[(\gamma, n)+2(\gamma, 2n)+(\gamma, pn)]$ to the cross section of theoretical importance, i.e., the total photoneutron cross section $\sigma_t = \sigma[(\gamma, n)+(\gamma, 2n)+(\gamma, pn)]$, without ambiguity and without the necessity of having to assume the nuclear level density.

A final factor is the degree of polarization achieved. By cooling the target to a temperature below that attainable with a He^3 refrigerator, it was possible to achieve approximately 80% of the maximum theoretical value for the alignment parameter $f_2(T)$ and, as a consequence, to observe 80% of the maximum possible difference between the polarized and unpolarized cross sections.

The technical aspects of the experiment fall into two main categories: (1) constructing the polarized holmium target, using the techniques of low-temperature physics, and (2) measuring its photonuclear cross section with the nearly monoenergetic photon beam from the Livermore linear accelerator. The techniques employed for making these photonuclear measurements have been used for previous studies conducted at the Livermore facility, and are described in detail elsewhere.[1,14,15] In Sec. IV, the experiment as a whole is described, then details of those components which were developed specifically for the experiment, e.g., the polarized target and a compatible neutron detector, are presented.

A. Experiment Layout

An over-all view of the experimental apparatus is shown in Fig. 1. Figure 1(a) is a drawing of the complete facility, showing the configuration of the beam-handling system and the location of the major components used for this experiment. Figure 1(b) is a more detailed view of the layout near the polarized target assembly.

The positron beam is produced between the first and second sections of the accelerator by pair production in a thick target of high atomic number, and is accelerated in the remaining two sections to any desired energy between 6 and 30 MeV. The beam transport system routes the resulting beam into the experimental cave through two 90° bends and focuses it on the annihilation target, a 0.375-in.-diam by 0.030 in.-thick beryllium disk. Energy analysis of the beam is accomplished after the first 90° bend by a two-jaw slit adjusted to pass positrons within ±1% of the central energy. The positrons that annihilate in the beryllium target produce a beam of photons, strongly peaked in the forward direction. This beam has an energy equal to that of the incident positron beam (plus 0.76 MeV from the rest mass of the annihilating pair) and an energy spread of approximately 3% FWHM. The residual positron beam that penetrates this target is swept into a beam dump where it is stopped in graphite.

Between the beryllium target and the cryostat assembly (a distance of approximately 8 ft), the photon beam passes through three lead collimators and a xenon-filled ion chamber. This ion chamber, which is the primary beam monitor, has been calibrated as a function of positron energy, so that it measures the absolute intensity of annihilation photons in the beam. At the center of the cryostat, where the holmium target is located, the collimated photon beam is approximately 0.875 in. in diameter and has an intensity of approximately 500 annihilation photons/sec.

The aperture through the polarizing magnets surrounding the holmium target was only 1.25 in. in diameter, so that careful alignment of the target assembly was necessary to prevent the photon beam from striking neutron-producing materials other than the target itself. Optical alignment was not possible because the cryostat was opaque; therefore, a technique of taking x-ray photographs with the photon beam itself was developed.

The neutron detector surrounding the cryostat was a large cylinder of polyethylene containing 48 BF_3 proportional counters. It had an over-all efficiency of approximately 25% for neutrons produced in the holmium target and was shielded on all sides by several layers of high-density boric acid bricks to reduce

---

[14] S. C. Fultz, R. L. Bramblett, J. T. Caldwell, and N. A. Kerr, Phys. Rev. **127**, 1273 (1962).

[15] R. L. Bramblett, J. T. Caldwell, R. R. Harvey, and S. C. Fultz, Phys. Rev. **133**, B869 (1964).

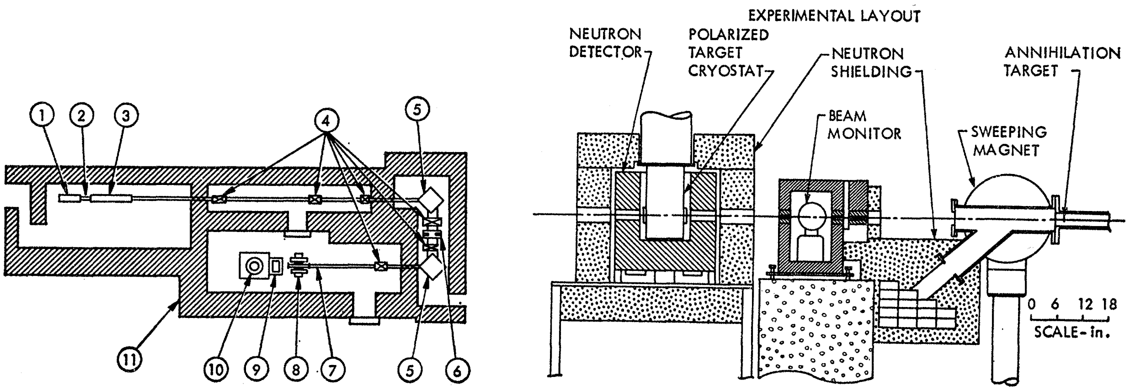

(a) (b)

FIG. 1. (a) Plan view of the Livermore linear accelerator facility. Electrons are accelerated in the first accelerator section (1), and strike a high atomic number target (2). Positrons produced in this target are accelerated in the remainder of the accelerator (3), then transported to the experimental area by two 90° bending magnets (5), quadrupoles (4), and a two-jaw energy slit (6). The positron beam strikes a thin beryllium target (7) producing forward-going photons that pass through the ion chamber (9) and polarized target assembly (10). The residual positron beam is diverted by the sweeping magnet (8). The accelerator and experimental caves are shielded by concrete walls (11). (b) Detailed elevation view of apparatus near polarized target. The 0.030-in.-thick×0.375-in.-diam beryllium annihilation target is suspended on threads in the center of a 4-in.-diam beam pipe. A larger section of evacuated beam pipe passes between the pole faces of the sweeping magnet, and is equipped with two thin aluminum windows. The swept positron beam strikes a graphite beam stop surrounded by boric acid bricks. The forward-going photon beam passes through a heavy lead box sitting on a concrete table in which the ion chamber and lead collimators are located. The cryostat houses the polarized target and is surrounded by the neutron detector and neutron shielding. Preamplifiers for the neutron detector are mounted beneath the detector.

neutron background originating from sources outside the cryostat. The performance and construction of this detector are described in detail in a subsequent section.

B. Procedure

During the experiment, four different cross sections of the holmium target were measured: A polarized and an unpolarized measurement with the alignment axis of the target oriented parallel to the incident photon beam, and two similar measurements with the target in a perpendicular orientation. The orientation of the target relative to the beam was changed by rotating both the holmium target and the polarizing magnet assembly about a vertical axis through the cryostat. To insure that the geometry was the same for both the polarized and the unpolarized measurements in a given orientation, both were made with the polarizing magnet operating and with no intervening disturbances of the cryostat, except that after a polarized measurement was completed, some helium gas was injected into the vacuum space surrounding the holmium target. This warmed the target to 4.2°K, thereby reducing its polarization to a negligible value.

Each cross-section measurement consisted of collecting data at approximately 30 different photon energies, a process requiring a total of about 48 h of accelerator time to complete. Each of these runs was conducted at a given energy in the following manner: The accelerator, operating at a repetition rate of 210 pulses/sec, was tuned to produce a 2-μsec pulse during which time (γ, n) and $(\gamma, 2n)$ processes occurred in the target. The neutron detector was then gated on for a period of 200 μsec after each beam pulse, and the number of such gates in which 0, 1, 2, 3, or 4 neutrons were detected during a run was recorded. The photon beam intensity was deliberately limited so that the probability of detecting two (γ, n) events in one gating interval was small. In this way, the number of $(\gamma, 2n)$ events occurring during a run could be obtained independently from the number of (γ, n) events by a stastical analysis of the number of gates in which 1, 2, 3, or 4 neutrons were detected. The beam intensity was monitored by measuring the total charge collected in the xenon-filled ion chamber during each run.

Since the positrons also produce bremsstrahlung in the beryllium annihilation target, the number of neutrons detected during a run includes some neutrons produced by these lower-energy photons. To obtain the neutron yield resulting from the annihilation photons alone, these neutrons must be subtracted. This was accomplished by reversing the polarity of the beam-handling system and retuning the accelerator so that electrons instead of positrons strike the beryllium target. Then, assuming that electrons and positrons of the same energy have the same bremsstrahlung spectrum, the neutrons produced by the electron bremsstrahlung provide the necessary subtraction. In order to normalize properly a positron run with an electron run at the same energy, the relative response of the ion chamber to the two different photon spectra must be known. This response has been measured by several independent techniques which give consistent results.[1]

C. Polarized Target

The polarized target was a 50-g sample of holmium metal composed of nine single crystals. Polarization was achieved by cooling the target to approximately 0.13°K in the presence of the 15-kOe magnetic field. This field is sufficient to orient the hyperfine fields in the holmium, which in turn polarize the nuclei.

Holmium was chosen as the target for this experiment because it is the most favorable nucleus from the standpoint of nuclear orientation. Its hyperfine interaction is the largest found in any element, corresponding to an effective field of over 9×10^6 G in the vicinity of a nucleus.[16] By orienting this field with an external field of a few kOe (i.e., magnetizing the holmium) one needs to cool the sample to only ~0.5°K to obtain substantial polarization. There are a number of papers in the literature describing the use of this technique to obtain nuclear polarization in holmium metal,[17–19] and nuclear alignment in holmium ethylsulfate.[20–22]

The nuclear properties of Ho^{165} are quite well suited to the experiment as well. It is monoisotopic and its intrinsic quadrupole moment is +7.6 b. Its photon absorption cross section in the giant resonance region is composed of two resolved peaks, permitting the change of each with polarization to be observed independently.

1. Polarization Method

The hyperfine interaction in holmium metal can be characterized by a spin Hamiltonian of the form

$$\mathcal{H} = A\mathbf{I}\cdot\mathbf{S} + P[I_Z^2 - \tfrac{1}{3}I(I+1)], \tag{9}$$

where A and P are the magnetic dipole and electric quadrupole hyperfine coupling constants, I is the nuclear spin, and I_Z is its projection on the quantization axis. Interactions with an externally applied magnetic field have been neglected because they are negligible for fields of a few kOe. Specific-heat measurements and elastic neutron scattering experiments give consistent values for A and P, A/k being 0.62°K[16,21,23,24] and P/k being 0.007°K.[16,24]

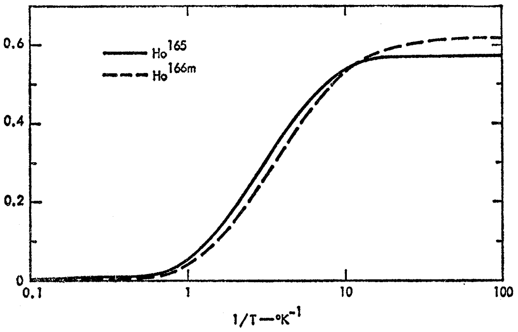

FIG. 2. Alignment parameter f_2 for Ho^{165} assuming $A/k=0.62$°K and $P/k=0.007$°K, and for Ho^{166m} assuming $A'/k=0.31$°K and $P'/k=0.00175$°K.

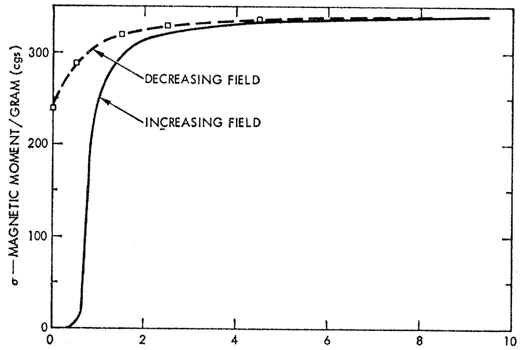

FIG. 3. Magnetization curve for a holmium single crystal along its $[10\bar{1}0]$ axis (see Ref. 26).

At a temperature T, the magnetic substate populations are given by the Boltzmann distribution

$$a_m = e^{-E_m/kT} \Big/ \sum_m e^{-E_m/kT}, \tag{10}$$

where E_m is the energy of the mth magnetic substate and k is Boltzmann's constant.

The alignment parameter f_2 of Tolhoek and Cox[12] is given by Eq. (5b), and is plotted for Ho^{165} in Fig. 2, assuming $I=\frac{7}{2}$, $A/k=0.62$°K, and $P/k=0.007$°K. As mentioned above, only the alignment parameter f_2 is important for this experiment because of the dipole nature of the giant resonance and because the photon beam is unpolarized. As Fig. 2 shows, the holmium is completely polarized at a temperature of approximately 0.05°K. For the temperature at which this experiment was performed, i.e., 0.13°K, $f_2 \approx 0.43$, or about 80% of this maximum value.

Below 20°K, holmium metal is ferromagnetic[25]; by applying an external field, the internal hyperfine field can be oriented along any one of six directions in the basal plane. These directions are the $[10\bar{1}0]$ crystalline axes, and are often referred to as the "easy axes of magnetization." Figure 3 shows a magnetization curve from Strandburg *et al.*[26] for a single crystal of holmium oriented along this axis. It shows that a few kOe is enough to completely magnetize the crystal, and the

---

[16] O. V. Lounasmaa, Phys. Rev. **128,** 1136 (1962).

[17] V. L. Sailor, R. I. Schermer, F. J. Shore, C. A. Reynolds, H. Marshak, and H. Postma, Phys. Rev. **127,** 1124 (1962).

[18] R. Wagner, P. D. Miller, T. Tamura, and H. Marshak, Phys. Rev. **139,** B29 (1965).

[19] J. S. McCarthy, T. R. Fisher, E. G. Shelley, R. S. Safrata, and D. Healey, Phys. Rev. Letters **20,** 491 (1968).

[20] D. A. Shirley, in *Annual Review of Nuclear Science,* edited by Emilio Segre (Annual Reviews, Inc., Palo Alto, Calif., 1966), Vol. 16.

[21] H. Postma, H. Marshak, V. L. Sailor, F. J. Shore, and C. A. Reynolds, Phys. Rev. **126,** 979 (1962).

[22] H. Postma, M. C. Eversdijk Smulders, and W. J. Huiskamp, Physica **27,** 245 (1961).

[23] B. Dreyfus, B. B. Goodman, A. Lacaze, and G. Trolliet, Acad. Sci. **253,** 1764 (1961).

[24] J. E. Gordon, C. W. Dempsey, and T. Soller, Phys. Rev. **124,** 724 (1961).

[25] S. Legvold, in *Rare Earth Research,* edited by Eugene V. Kleber (The Macmillan Co., New York, 1961).

[26] D. L. Strandburg, S. Legvold, and F. H. Spedding, Phys. Rev. **127,** 2046 (1962).

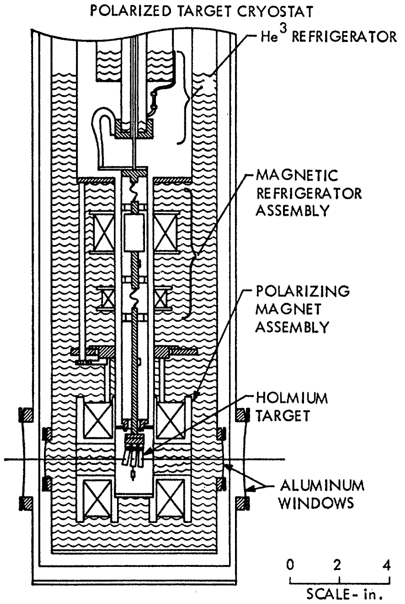

FIG. 4. The polarized target cryostat. A He^3 refrigerator cools the target to ~0.3°K, and a stage of magnetic refrigeration cools it to its operating temperature 0.13°K. A 15-kOe field magnetizes the nine holmium crystals in the target. Both the polarizing magnet and the magnetic refrigerator can be rotated 90° about a vertical axis, so that the photon beam can be oriented parallel to or perpendicular to the target quantization axis.

macroscopic magnetic moment measured in this condition agrees with what one would expect if the entire hyperfine field were aligned in this direction.

2. *Cryostat and Target Assembly*

Figure 4 shows the cryostat, target, and polarizing magnet used for the experiment. The cryostat consisted of a He^3 refrigerator that was capable of maintaining a temperature of 0.34°K with no heat input. In it, He^3 was liquefied by contact with a bath of He^4 at 1°K, throttled across a sintered stainless steel plug, then cooled to 0.34°K by reducing its saturation vapor pressure.[27]

An additional stage of cooling was provided between the He^3 refrigerator and the target. This consisted of a recycling magnetic refrigerator of the type described by Daunt *et al.*[28,29] It operated by thermally connecting a pill of ferric ammonium alum alternately to the He^3 refrigerator and then to the holmium target through two superconducting lead heat switches. While the salt was connected to the He^3 refrigerator, it was magnetized and allowed to come to thermal equilibrium with the He^3. Then it was demagnetized and connected to the holmium target so that heat flowed into the salt. This stage of refrigeration was operated continuously, each cycle taking about 10 min, so that the holmium reached a final temperature of approximately 0.13°K. Operating and construction details of this magnetic refrigeration stage have been described.[30]

The target assembly consisted of nine single crystals approximately $\frac{1}{4}$ in. in diameter and $\frac{3}{4}$-in. long, arranged in a square array. One end of each crystal was soldered to a small copper base at an angle such that one of its axes of magnetization lay in the plane perpendicular to the axis of the base. This required tilting the crystals by varying amounts from 1° to 12°, since they did not possess the same crystalline orientation relative to their geometry. The orientation of the crystalline axes in each crystal was determined by x-ray diffraction before mounting. The nine crystal bases were then attached to a common copper block in such a way that all the crystals had a mutual easy axis of magnetization. Details of the target construction are included in Ref. 30.

To magnetize the target, a split-pair superconducting solenoid capable of producing a 25-kOe field at its center was used. It had a $1\frac{1}{4}$-in.-diam axial hole and also a $1\frac{1}{4}$-in.-diam hole perpendicular to the field. It was mounted in the helium Dewar in such a way that it could be rotated 90° about a vertical axis, permitting the incident photon beam to be oriented either perpendicular to or parallel to the field. Since the field had to be applied along a particular axis of the holmium crystals, they were rotated with the magnet. This was accomplished by a separate mechanical control, which permitted the target and magnetic refrigerator assembly to be rotated by 90° or to be lifted so that the target was removed from the beam when background measurements were taken. During the experiment the magnet was operated in the persistent mode, and the field was limited to 15 kOe to reduce somewhat the mechanical stresses on the target.

3. *Measurement of Polarization*

If the temperature of the holmium is known and it is assumed to be completely magnetized, all of the alignment parameters, f_2 in particular, can be calculated using the Boltzmann distribution for the relative populations of the magnetic substates and the formulas in Ref. 12.

We have, however, made a more direct measurement of f_2 in the case of Ho^{165}. The technique[31] consists of inducing some Ho^{166m} activity in the holmium target, and then measuring the anisotropy of the γ rays emitted from its decay. In this way, the alignment parameter for the Ho^{166m}, f_2', can be determined and, by knowing the spins and hyperfine interaction constants of the two nuclei, f_2 for Ho^{165} can be computed. Such a technique has the advantage that both nuclei are in very similar crystalline and thermal environ-

---

[27] E. Ambler and R. B. Dove, Rev. Sci. Instr. **32**, 737 (1961).

[28] J. G. Daunt, Proc. Phys. Soc. (London) **70**, 641 (1957).

[29] C. V. Heer, C. B. Barnes, and J. G. Daunt, Rev. Sci. Instr. **25**, 1088 (1954).

[30] M. A. Kelly, University of California Lawrence Radiation Laboratory Report No. UCRL-50421, 1968 (unpublished).

[31] D. A. Shirley (private communication).

ments; consequently, neither the temperature nor the magnetization of the target needs to be known precisely in order to determine f_2.

To induce the required Ho^{166m} activity, the central crystal (weighing 5.2 g) in the nine-crystal target was placed in a 2×10^{12}-n/cm^2 sec thermal-neutron flux at the Livermore reactor for 30 h. After allowing the 27-h activity of Ho^{166} to decay, the crystal possessed a suitable amount of Ho^{166m} activity (5 mR/h at 3 in.) to enable accurate measurements of its γ-decay spectrum to be made using a Ge(Li) detector.

The pertinent portion of the decay scheme for Ho^{166m} is shown in Fig. 5.[32] Assuming the β decay is allowed, the alignment parameter f_2' of the 1786-keV level is related to that of the ground state of Ho^{166m} by the relation[33]

$$N_2(I_0)f_2'(I_0)=N_2(I_1)f_2'(I_1), \tag{11}$$

where $N_2(I_i)=I_i/(2I_i-1)$, I_0 is the spin of the ground state of Ho^{166m}, and I_1 is the spin of the 1786-keV level in Er^{166}. Thus, by measuring the anisotropy of the succeeding γ transition, one can compute the initial polarization using the formulas given by Cox and Tolhoek.[34] For a pure $E1$ transition from a state I to a state $(I-1)$, such as the 710-keV line in Ho^{166m},

$$W(\phi)=2[1+\tfrac{3}{2}N_2f_2P_2(\cos\phi)], \tag{12}$$

where $W(\phi)$ is the angular distribution of γ rays, and φ is the angle of the detector measured from the polarization axis. Hence, by measuring the photon flux along the quantization axis ($\phi=0°$) when the target is polarized [$W(\phi)$ cold] and unpolarized [$W(\phi)$ warm], the value of f_2' for the ground state of Ho^{166m} is given by

$$f_2'=\frac{2}{3N_2}\left[\frac{W(\phi)\text{ cold}}{W(\phi)\text{ warm}}-1\right]. \tag{13}$$

From γ-anisotropy measurements on a transition that is a mixture of $E2$ and $M1$, such as the 810-keV line in Ho^{166m}, one can obtain a relation between f_2' and f_4'. From Eq. (3) of Ref. 33, one has for such a transition from a state I_i to (I_i-1),

$$\begin{aligned}W(\phi)=2\Bigg\{1+\frac{1}{14}\Bigg[&21a_1^2+42\left(\frac{15I_i-1}{I_i+1}\right)^{1/2}a_1a_2\\&+15\left(\frac{I_i-5}{I_i+1}\right)a_2^2\Bigg]N_2f_2'P_2(\cos\phi)\\&+10\left(\frac{2I_i-3}{I_i+1}\right)a_2^2N_4f_4'P_4(\cos\phi)\Bigg\},\end{aligned} \tag{14}$$

where

$$N_k=2^{k/2}I[(2I-k)!/2I!],$$

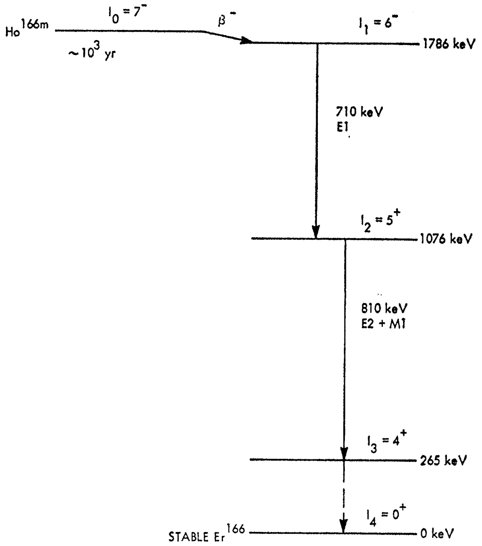

FIG. 5. The decay scheme of Ho^{166m}. Both the 710- and 810-keV transitions were used to measure the target polarization. The 810-keV line was determined to be 4% $M1$ from the data of Shirley in Ref. 20.

and a_1 and a_2 equal the dipole and quadrupole mixtures, normalized so that $a_1^2+a_2^2=1$.

Although only f_2 is needed to interpret the photonuclear results, this relation provides an approximate measurement of the target temperature from the ratio of f_4'/f_2'. This ratio is a function of temperature, and since it is independent of the magnitude of the isotropic part of the distribution of γ rays emitted from the target, one can obtain an approximate indication of temperature even though the target is not magnetically saturated. Solving Eq. (14) for this ratio using the anisotropy of the 810- and 710-keV lines in Ho^{166m} gives

$$\begin{aligned}\frac{f_4'}{f_2'}=0.0427&\\&\times\left\{4.06\,\frac{[(W(\phi)\text{ cold}/W(\phi)\text{ warm})-1]_{810\text{ keV}}}{[(W(\phi)\text{ cold}/W(\phi)\text{ warm})-1]_{710\text{ keV}}}-1\right\}\\&\times\frac{P_2(\cos\phi)}{P_4(\cos\phi)}.\end{aligned} \tag{15}$$

Figure 6 is a plot of this ratio as a function of temperature.

To relate the value of f_2' for Ho^{166m} to f_2 for Ho^{165}, the two nuclei are assumed to be in thermal equilibrium with each other and in the same crystalline environment. Then using the Boltzmann distribution for a target at temperature T, the ratio of f_2 to f_2' is calculated from the relation

$$\frac{f_2}{f_2'}=\frac{I'^2[\sum_m m^2a_m-\frac{1}{3}[I(I+1)]]}{I^2[\sum_m m'^2a_m'-\frac{1}{3}[I'(I'+1)]]}, \tag{16}$$

---

[32] S. B. Burson, P. F. A. Goudsmit, and J. Konijn, Phys. Rev. **158,** 1161 (1967).

[33] C. D. Hartogh, H. A. Tolhoek, and S. R. deGroot, Physica **20,** 1310 (1954).

[34] J. A. M. Cox and H. A. Tolhoek, Physica **19,** 673 (1953).

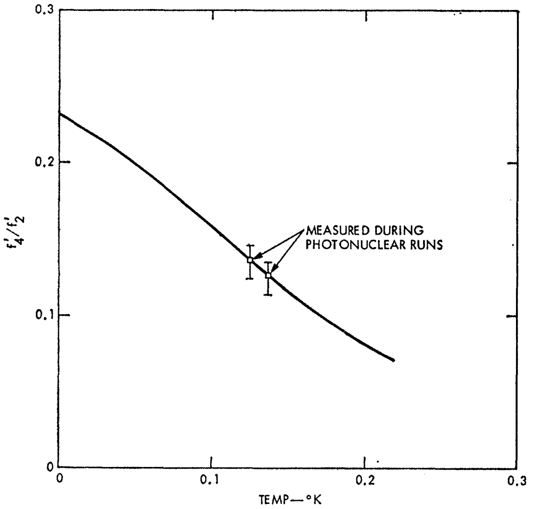

FIG. 6. Calculated value of the ratio of f_4'/f_2' from Eq. (15) (the primes refer to values for the Ho^{166m} nucleus). The two points with error bars are the values of this ratio measured during the photonuclear runs. The temperature was thus determined to be ~0.13°K.

where the primes are the parameters for the Ho^{166m} nuclei, I is the nuclear spin, m is the magnetic substate quantum number, and the a_m's are the magnetic substate population, defined in Eq. (10), for the target temperature T.

Both spins are well known, $I=\frac{7}{2}$ for Ho^{165} and $I=7$ for Ho^{166m}. The hyperfine structure (hfs) constant for Ho^{166m} in holmium ethylsulfate has been measured by Postma *et al.*[35] to be $A/k=0.24\pm0.02$°K, although the stated uncertainty of this measurement might be too small because the decay scheme of Ho^{166m} was not known correctly. There are no measurements of this constant for Ho^{166m} in metal, but A/k for Ho^{165} in holmium ethylsulfate was determined to be 0.48°K by Baker and Bleaney.[36] The fact that A/k for Ho^{165} in the metal is 0.62°K (20% higher than in the ethylsulfate) indicates that the hyperfine field is higher in the metal, so A/k for Ho^{166m} in metal should be 0.31 ± 0.03°K. The ratio f_2/f_2' is plotted in Fig. 7 and is seen to be relatively independent of temperature, so that the target temperature T need not be known with great precision.

Two sets of γ-anisotropy measurements were made during the experiment, one after completing the photonuclear measurements in which the photon beam was oriented perpendicular to the target quantization axis, and the other following the parallel photonuclear measurements. The former set was made using a single Ge(Li) detector positioned along the target quantization axis; for the latter set, an additional detector was positioned perpendicular to this axis.

For all these measurements, the position of the magnet assembly and target was not disturbed between the photonuclear measurements and the corresponding γ-anisotropy measurements.

The target temperature, however, had to be raised to 4.2°K during each set of photonuclear measurements, so that recooling was necessary in order to measure the γ anisotropy. Since care was taken to reproduce the original temperature (indicated by a secondary thermometer mounted on the target), the polarization during the photonuclear measurement should be the same as that determined by the corresponding γ-anisotropy measurement. A summary of these γ-anisotropy measurements taken during the photonuclear experiment is shown in Table I. The values listed in the table for f_2' were calculated from the anisotropy of the 710-keV line using Eq. (13), and the temperatures listed were obtained from the ratio f_4'/f_2' from Eq. (15). These temperatures are consistent with those measured by the secondary thermometers in the cryostat, $T=0.11\pm0.03$°K.

The uncertainties listed reflect the statistical uncertainties in the γ-anisotropy measurements, and not the uncertainty in the value of A/k and P/k for Ho^{166m} which were taken to be 0.31 and 0.00175°K, respectively. This value of P/k assumes that Ho^{165} and Ho^{166m} have the same intrinsic quadrupole moment.

To obtain a value for f_2, the alignment parameter for the Ho^{165} target as a whole, Eq. (16) is evaluated using the average temperature determined by the γ-anisotropy measurements $T=0.13$°K. The value so obtained is then corrected for: (a) errors in the orientation of the crystalline axes of each of the nine single crystals relative to the polarization axis of the target, and (b) the nonuniformity of the magnetization throughout the target (see Ref. 30 for details). These corrections indicate that the value of f_2 one obtains from Eq. (16) is 3% too low. Thus, the corrected values of f_2 obtained from the γ-anisotropy measurements for the entire Ho^{165} target are $f_2=0.44\pm0.05$ (applicable to the parallel photonuclear measurements) and $f_2=0.42\pm$

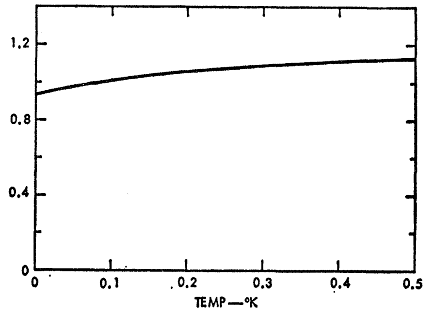

FIG. 7. The calculated ratio of f_2 (the alignment parameter of the Ho^{165}) to f_2' (the alignment of Ho^{166m}) as a function of temperature. For Ho^{165} it is assumed $A/k=0.62$°K, $P/k=0.007$°K, and for Ho^{166m} $A/k=0.31$°K, $P/k=0.00175$°K is used.

---

[35] H. Postma, A. R. Miedema, and M. C. Eversdijk Smulders, Physica **25**, 671 (1959).

[36] J. M. Baker and B. Bleaney, Proc. Roy. Soc. (London) **245**, 156 (1958).

TABLE I. γ anisotropy measurements.

Photonuclear runs	ϕ (deg)	$W(\phi)$ cold[a]/$W(\phi)$ warm 710-keV line	810-keV line	Calculated[b] f_2'	Calculated[c] T(°K)
Photon beam ‖ polarization axis	0	1.361±0.015	1.37±0.015	0.45±0.02	0.125±0.01
	90	0.839±0.014	1.06±0.015	0.40±0.03	
Photon beam ⊥ polarization axis	0	1.334±0.02	1.33±0.02	0.41±0.03	0.135±0.01

[a] Defined in Eq. (13).
[b] Calculated using Eq. (13).
[c] Calculated using Eq. (15).

0.05 (applicable to the perpendicular photonuclear measurements). These values were used in the data analysis. Their stated uncertainties have been increased to include the uncertainty in the hfs constants A/k and P/k for Ho^{166m}.

D. Neutron Detector

The neutron detector, which surrounded the lower portion of the cryostat, consisted of 48 BF_3 proportional counters imbedded in a cylindrical polyethylene moderator. Its mechanical details and the placement of the BF_3 counters in the moderator are given in Ref. 30. The counter tubes have a diameter of 1 in. and an active length of 20 in., and are filled with B^{10}-enriched BF_3 to a pressure of 167-cm Hg. The detector is divided electrically into quadrants with each 12-tube segment having its own high-voltage distribution network and preamplifier. To minimize electrical pickup and to reduce wiring problems, the tubes and the preamplifiers were mounted directly on the high-voltage distribution boxes, forming four integral assemblies.

The efficiency of the detector was determined using three (α, n) sources (PoLi, mock fission, and PuBe) and neutrons from the spontaneous fission of Cf^{252}. The mock fission and PoLi sources were calibrated in a $MnSO_4$ bath; the PuBe source was calibrated by comparing it to a similar source calibrated in such a bath; and the Cf^{252} source was calibrated directly by measuring its fission rate. For these measurements, the lower sections of the cryostat including the polarizing magnet assembly were placed in the detector to simulate the actual conditions of the experiment. The sources were placed in the space normally occupied by the holmium target, so that the only major difference that existed between the operating conditions and these efficiency measurements was the absence of liquid helium for the latter. Monte Carlo calculations were made to estimate the effect of the helium on the neutron detector efficiency, and these indicated it was negligible. Subsequent measurements confirmed this calculation.

The time response was measured by using the spontaneous fission of Cf^{252}. A 1024-channel time analyzer was started when a fission fragment was detected in a solid-state detector upon which the Cf^{252} was mounted, and stopped by the fission-produced neutrons. Thus, the time spectrum for the detection of fission-produced neutrons was accumulated. By using the value $\bar{\nu} = 3.78$,[37] the efficiency for the Cf^{252} neutrons was also calculated.

For the data analysis, the gated efficiency given by the solid line in Fig. 8 was used. The average neutron energy was determined as a function of the incident photon energy from the unpolarized data shown in Fig. 1, which was taken with a neutron detector having four concentric rings of BF_3 tubes. The efficiency of these rings vary relative to each other with neutron energy and, by a technique described elsewhere,[38] the average energy for neutrons resulting from (γ, n) and $(\gamma, 2n)$ reactions was obtained.

During the experiment, the detector was gated on 5 μsec after the beam pulse from the linear accelerator for a period of 200 μsec. The ratio of gated-to-ungated efficiency is

$$\epsilon_{\text{gated}}/\epsilon_{\text{ungated}} = \left(\int_5^{205\mu\text{sec}} \eta(t)\,dt\right) \bigg/ \left(\int_0^{\infty} \eta(t)\,dt\right) = 0.80\,, \tag{17}$$

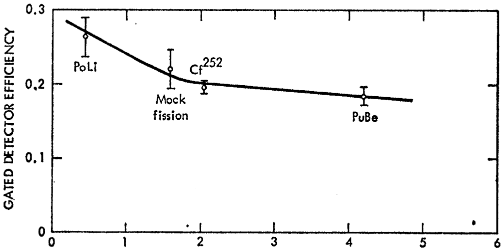

FIG. 8. The gated efficiency of the neutron detector measured with the cryostat and polarizing magnet in place. The sources used for these measurements are shown in the figure, and the solid line is the value used for the data analysis. The neutron energy for a given incident photon energy was determined for the photonuclear data using the ring ratio technique described in Ref. 38.

---

[37] S. C. Fultz, J. T. Caldwell, B. L. Berman, R. L. Bramblett, M. A. Kelly, H. D. Wilson, M. S. Coops, R. W. Lougheed, J. E. Evans, and R. W. Hoff, Phys. Rev. **152**, 1046 (1966).

[38] J. T. Caldwell, R. L. Bramblett, B. L. Berman, R. R. Harvey, and S. C. Fultz, Phys. Rev. Letters **15**, 976 (1965).

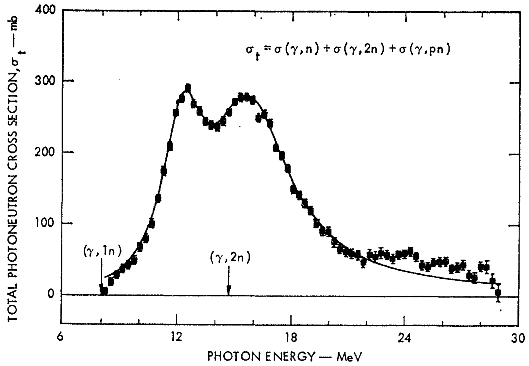

FIG. 9. Total photoneutron cross section for unpolarized Ho^{165}. This measurement was made on a 191-g sample of holmium metal using the detector and techniques described in Ref. 1. The solid line is a two-component Lorentz curve fit to the unpolarized data of Fig. 10.

where $\eta(t)$ is the time response of the detected neutrons. If the measured time spectrum is assumed to be independent of neutron energy, an assumption which is justified by the short thermalization time in hydrogenous materials, the ratio just calculated is a constant, and one obtains the gated efficiency shown in Fig. 8.

IV. RESULTS AND DISCUSSION

As mentioned in the last section, the following four cross sections were measured with the target in the cryostat:

(1) target polarized, ($T\cong 0.13°K$) its quantization axis perpendicular to the photon beam;
(2) target unpolarized, ($T\cong 4.2°K$) oriented as in (1);
(3) target polarized, ($T\cong 0.13°K$) its quantization axis parallel to the photon beam; and
(4) target unpolarized, ($T=4.2°K$) oriented as in (3).

Since the holmium target had an irregular shape, the photon beam did not necessarily illuminate the same mass of holmium in the two different orientations, so that measurements (2) and (4) were made to provide a way of normalizing the two polarized runs (1) and (3). In addition, these two unpolarized measurements were normalized to the more detailed absolute measurement of the total photoneutron cross section for Ho^{165} shown in Fig. 9 to determine the absolute cross sections for the polarized measurements.

All of the cross sections presented have been corrected for: (a) neutron multiplicity, (b) neutrons produced by bremsstrahlung photons, (c) the variation of detector efficiency with neutron energy, and (d) neutrons produced by sources other than the holmium target. Corrections (a) and (b) were made in the manner outlined in Sec. III B, and (c) by using the procedure discussed in Sec. III D. The error bars on the data reflect all of these corrections except (c) those attributed to variations in the neutron detector efficiency. The latter, however, affect the results only secondarily through the multiplicity calculations, since the detector efficiency was not used to determine an absolute scale for the cross section.

The last of these corrections (d) for neutrons produced by sources other than the holmium target was made by using a measurement of the neutron yield with the holmium target lifted out of the beam. This was found to be less than 10% of the target-in cross section below 18 MeV, and less than 20% at 21 MeV.

A. Unpolarized Data

Figure 9 shows the total photoneutron cross section of unpolarized holmium used to normalize the data taken with the target in the cryostat [measurements (2) and (4) above]. This cross section was determined from a 191.5-g sample of holmium metal (99% purity) using the detector and techniques described in Ref. 1, and supersedes a previous measurement of the holmium cross section made at this laboratory.[10] The energy spread of the photon beam during the measurement was not greater than 3% FWHM (the measured width of the 17.2-MeV resonance in O^{16}). To obtain an absolute cross section, the photon flux was determined with an 8-in.×8-in. NaI γ spectrometer with a known response function, and the efficiency of the neutron

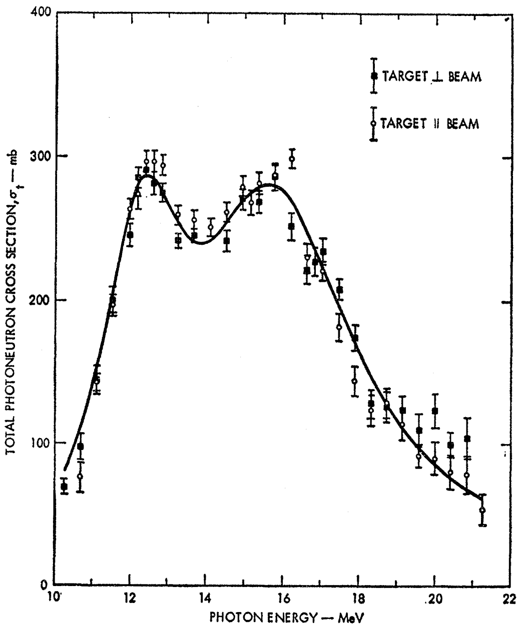

FIG. 10. The two unpolarized cross sections taken with the target oriented parallel to the photon beam and perpendicular to the beam. The target temperature during these measurements was 4.2°K; otherwise, the conditions were identical to those during the polarized runs. The solid line is a two-component Lorentz curve fit to the data, the parameters of which are given in Table III B.

detector was measured as a function of neutron energy using a number of calibrated sources. The data were analyzed by the "ring-ratio" technique[38] in which one obtains the average neutron energy for (γ, n) and $(\gamma, 2n)$ events independently as a function of photon energy. From these values of the average neutron energy, the efficiencies for detecting (γ, n) and $(\gamma, 2n)$ events were computed using the source calibration, and were used to analyze the data.

The resulting total photoneutron cross section has been corrected for photon absorption in the holmium sample and for neutrons produced by bremsstrahlung photons. Systematic uncertainties in the absolute cross section arising from the neutron detector calibration and from the above-mentioned corrections are judged to be less than ±7%.

Figure 10 shows the total neutron production cross section $\sigma_t = \sigma[(\gamma, n) + (\gamma, 2n) + (\gamma, np)]$ for the two unpolarized runs with the holmium target in the cryostat ($T = 4.2$°K). Since the shape of the unpolarized cross section is well known from the more detailed data just described (Fig. 9), these measurements were not made in great detail; just enough data were taken to enable good normalization. When analyzed in an identical manner, the integrated cross section for the perpendicular orientation [measurement (2)] was 2% higher than that for the parallel orientation [measurement (4)], presumably because a larger mass of holmium was in the photon beam for the former measurement. Consequently, all of the data taken in the parallel orientation [measurements (3) and (4)] were multiplied by 1.02 so that the two unpolarized cross sections agreed with each other.

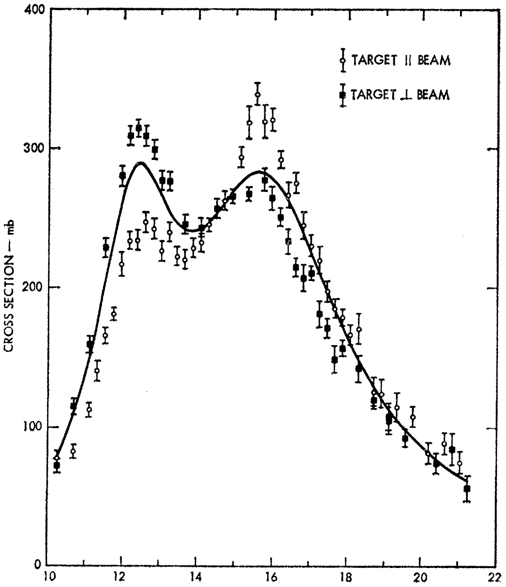

FIG. 11. The cross sections measured with the holmium target polarized parallel to the photon beam and perpendicular to the photon beam. The solid line is the two-component Lorentz curve fit to the unpolarized data.

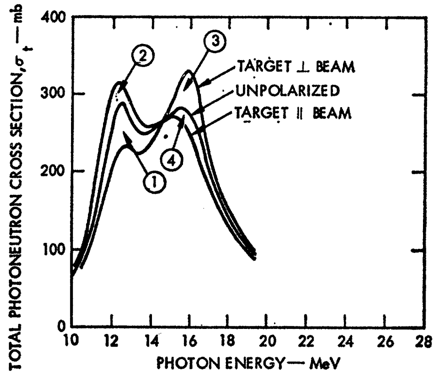

CROSS SECTIONS INTEGRATED FROM 8 TO 20 MeV (IN MeV mb)

	TARGET QUANTIZATION	
	AXIS ∥ PHOTON BEAM	AXIS ⊥ PHOTON BEAM
UNPOLARIZED	2084 ± 21	2082 ± 22
POLARIZED	2060 ± 15	2092 ± 18
UNPOLARIZED DATA OF FIG. 1	2081 ± 10	

MEASURED ANISOTROPY FROM 10.5 TO 20.5 MeV (IN MeV mb)

AREA ① = 110 ± 12	AREA ③ = 90 ± 18
AREA ② = 52 ± 12	AREA ④ = 57 ± 18
① + ② = 162 ± 11	③ + ④ = 147 ± 16

FIG. 12. The anisotropy observed in the photoneutron measurements and their integrated cross sections.

To obtain an estimate of how well the shape of these unpolarized cross sections agree with that of the more detailed data, the same solid curve is plotted in both Figs. 9 and 10. This curve is a least-squares fit of two Lorentz curves to measurements (2) and (4) in which the widths and energies were held constant. This and other fits to the data will be considered in more detail subsequently.

B. Polarized Target Data

Figure 11 shows the two total photoneutron cross sections taken with the target polarized. Also shown is the two-component Lorentz-curve fit to the unpolarized data just discussed. The data agree qualitatively with the predictions of the collective model in that the 12-MeV resonance is enhanced when the target is oriented perpendicular to the beam and is diminished in the parallel orientation, while the reverse is true for the 16-MeV resonance. A summary of the conditions under which these measurements were made is given in Table II.

The consistency of the data can be checked in two ways. First, if the dipole sum rule is valid, the integrated photon absorption cross section will be independent of nuclear orientation. Integrating the four sets of data to 20 MeV, one finds that they do in fact agree to within the experimental error limits (see Fig. 12).

TABLE II. Summary of the conditions under which the photonuclear measurements were made. (θ is the angle between the target polarization axis and the incident photon beam.)

	Target polarized $\theta=0°$	Target polarized $\theta=90°$	Target unpolarized
Alignment parameter of Ho^{166m} in central crystal, f_2'	0.43±0.03	0.41±0.03	<0.005
Corrected alignment parameter for Ho^{165}, f_2	0.44±0.05	0.42±0.05	<0.005
Temperature of target (°K)	0.125±0.015	0.135±0.015	4.2
Applied field (kOe)	15	15	15

A second check on the consistency of the data can be obtained using Eq. (8), which requires that for a dipole process the anisotropy observed for $\theta=90°$ be one-half the magnitude of that seen for $\theta=0°$. Referring to Fig. 12, this is also seen to be true within experimental errors.

Parameters describing least-squares fits of two Lorentz curves to these data as well as to the unpolarized cross sections presented in III A above are given in Table III. Two types of fits are presented: The first are free fits in which the amplitude, width, and energy of each Lorentz curve was allowed to vary; for the second, the width and energy of each were held fixed at the values giving the best over-all fit for the three different polarization conditions. Fits to the polarized cross sections using the latter set of parameters are shown in Fig. 13.

C. Intrinsic Cross Sections

From Eq. (8), the relationship between the intrinsic modes of the giant resonance $\sigma_{\|}$ and $\sigma_{\perp}$ and the measured cross sections $\sigma(0°)$ and $\sigma(90°)$ are

$$\sigma_{\|}=1.146[1.292\sigma_t(90°)-\sigma_t(0°)],$$

$$\sigma_{\perp}=0.804[1.829\sigma_t(0°)-\sigma_t(90°)].$$

(These relations assume the alignment parameter $f_2=0.42$ for the measurement at $\theta=90°$ and $f_2=0.44$ for the one at $\theta=0°$.) Using these equations, the two intrinsic cross sections were computed and are shown in Fig. 14. For those photon energies at which both $\sigma(0°)$ and $\sigma(90°)$ were measured, the intrinsic cross sections were calculated directly from the data. There were, however, a few energies at which only one of these two quantities was measured. At these energies a value for the missing quantity was obtained by interpolation from neighboring points.

D. Comparison of Results with Collective Theories

In this section, the experimental results are compared with two collective models: (1) an elementary model that regards the giant dipole resonance as resulting

TABLE III. Parameters for the two-component Lorentz curve fits[a] to the polarized and unpolarized total cross sections. The fitting range is from 10.6 to 18.0 MeV.

	E_1 (MeV)	σ_1 (mb)	Γ_1 (MeV)	E_2 (MeV)	σ_2 (mb)	Γ_2 (MeV)
A. Free fits: all parameters allowed to vary						
Unpolarized data of Fig. 1	12.28±0.02	216±5	2.51±0.09	15.79±0.04	249±3	4.99±0.20
Polarized, beam ∥ target	12.37±0.04	173±6	2.43±0.15	15.76±0.04	291±4	4.28±0.16
Polarized, beam ⊥ target	12.28±0.03	244±7	2.46±0.11	15.63±0.06	233±4	4.94±0.23
Unpolarized, ∥ and ⊥ data combined	12.32±0.04	214±10	2.32±0.17	15.71±0.08	257±5	5.04±0.36
B. Fits with $E_1=12.28$ MeV, $\Gamma_1=2.5$ MeV, $E_2=15.78$ MeV, $\Gamma_2=5.0$ MeV		σ_1 (mb)			σ_2 (mb)	
Unpolarized data of Fig. 1		215±2			249±2	
Polarized, beam ∥ target		152±4			281±4	
Unpolarized, beam ∥ target		221±6			256±5	
Polarized, beam ⊥ target		250±3			229±3	
Unpolarized, beam ⊥ target		212±5			249±5	

[a] $\sigma_t(E)=\sum_{i=1}^{2}E^2\Gamma_i^2\sigma_i/[(E^2-E_i^2)^2+E^2\Gamma_i^2]$.

from the motion of one-dimensional harmonic oscillators oriented along and perpendicular to the direction of the incident photon beam; and (2) the dynamic collective model of Danos and Greiner.[4] For both of these comparisons, Eq. (8) was used for the relationship between the absorption cross section and the nuclear matrix elements, assuming that the resonance shapes for the vibrational modes are Lorentzian, a shape that characterizes the giant resonance in spherical nuclei quite well.

The predictions of these two models are plotted together with the present experimental results in Figs. 15 and 16. The former figure shows the total photoneutron cross sections calculated from the models for the polarization conditions achieved during this experiment; the latter shows the intrinsic cross sections derived from the models. These figures show that both models explain the general dependence upon nuclear orientation of the giant resonance; i.e., the lower energy peak of the giant resonance is enhanced when the target polarization axis is perpendicular to the incident photon beam, while the higher energy peak is enhanced when the target is oriented parallel to the photon beam. Thus, the association of a dipole vibration along the nuclear symmetry axis with the lower energy peak (and transverse vibrations with the higher energy peak) that its implicit in both models is in agreement with the experimental results. In some details, however, notably in the magnitude of the cross-section anisotropy and in the shape of the intrinsic cross sections, there is some disagreement between the models and the experimental results. These are discussed below.

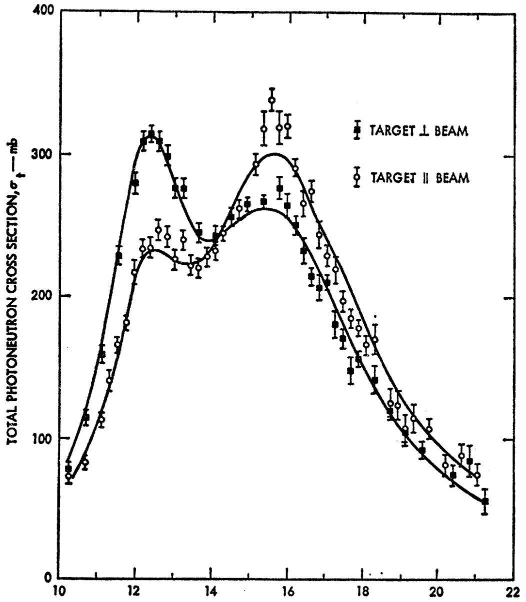

FIG. 13. Two-component Lorentz curve fits to the polarized data shown in Fig. 11. The parameters for these fits are listed in Table III.

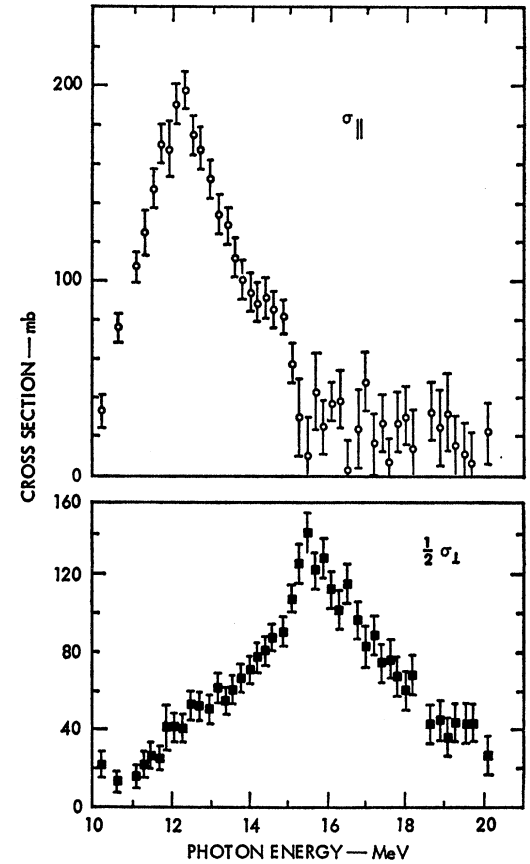

FIG. 14. The intrinsic cross sections for Ho^{165}. The cross section $\sigma_{\parallel}$ is associated with vibrations along the nuclear symmetry axis. One-half $\sigma_{\perp}$ is half the cross section associated with vibrations perpendicular to the symmetry axis. The error bars represent statistical errors, and not those due to the uncertainty of f_2.

1. *Elementary Model*

To calculate the effect of nuclear orientation from the elementary model, the parameters from the two-component Lorentz curve fit to the unpolarized cross section were used to define the model parameters (Table III A). This Lorentz fit agrees well with the model in several aspects. For example, the mean energy of the giant dipole resonance calculated from these parameters agrees with Eq. (1), if a nuclear symmetry energy constant $K=27.8$ MeV is used and the ratio between the central energies of the two-component curves is within 1% of that predicted by Eq. (2). Since the model does not specify the widths of the resonances, they are provided empirically from the Lorentz parameters.

There is, however, one way in which this two-component Lorentz curve fit to the unpolarized data does not agree with the model. One expects, if the TRK dipole sum rule is valid, that the integrated cross section $\int\sigma_t dE$ is a function only of N, Z, and A, and is thus independent of nuclear orientation. This requires that the integrated cross section of each vibrational mode be equal, so that $\int\sigma_{\perp}dE=2\int\sigma_{\parallel}dE$. For the Lorentz

Table IV. Calculated Lorentz parameters for polarized Ho (elementary model).

	E_1 (MeV)	Γ_1 (MeV)	σ_1 (mb)	E_2 (MeV)	Γ_1 (MeV)	σ_2 (mb)
Two-component Lorentz curve fit to the unpolarized data	12.28	2.5	215	15.78	5.0	249
$\sigma_t(0°)$ (Photon beam ‖ target)	12.28	2.5	138	15.78	5.0	294
$\sigma_t(90°)$ (Photon beam ⊥ target)	12.28	2.5	252	15.78	5.0	228

fits to the data, however, where $\int\sigma_{||}dE=\frac{1}{2}\pi\sigma_1\Gamma_1$ and $\int\sigma_\perp dE=\frac{1}{2}\pi\sigma_2\Gamma_2$ (σ_1, σ_2, Γ_1, and Γ_2 are found in Table III) one obtains $\int\sigma_\perp dE=2.3\int\sigma_{||}dE$. Considerably poorer fits to the data are obtained if $\int\sigma_{||}dE$ is restricted to equal $2\int\sigma_\perp dE$, so that one might conclude that the Lorentzian shapes only approximate the cross sections of the vibrational modes.

Ignoring this discrepancy for the moment, the lower-energy Lorentz curve is assumed to represent the cross section of the vibration along the nuclear symmetry axis ($\sigma_{||}$), while the higher energy curve is assumed to represent the two degenerate vibrations perpendicular to that axis ($\sigma_\perp$). The cross sections for a polarized target are then calculated from $\sigma_{||}$ and $\sigma_\perp$ using Eq. (8). The solid curves plotted in Fig. 15 and the corresponding parameters listed in Table IV were obtained in this manner.

If one compares the parameters of Table IV with the two-component Lorentz fits to the polarized data cross sections obtained experimentally (Table III), it is seen that the amplitudes of the two peaks in the giant resonance do not change as much going from one polarization condition to another as the model predicts. Quantitatively, this can be seen in a way that is least sensitive to statistical uncertainties in the data by integrating the difference between the cross sections obtained for the two different polarization conditions. This difference A_t is

$$A_t=\int_{10.5\,\mathrm{MeV}}^{20.5\,\mathrm{MeV}} |\,\sigma_t(0°)-\sigma_t(90°)\,|\,dE, \qquad (18)$$

where $\sigma_t(\theta)$ is the total photoneutron cross section $\sigma[(\gamma,n)+(\gamma,2n)+(\gamma,pn)]$ when the target is polar-

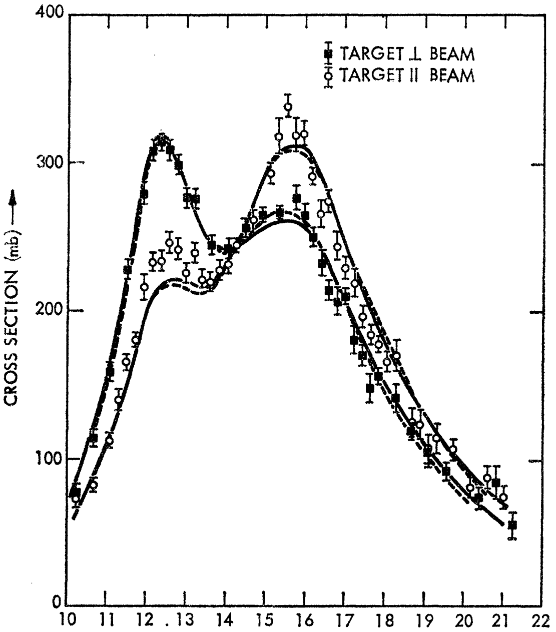

Fig. 15. Cross sections calculated from the elementary (solid lines) and dynamic (dashed lines) collective models for the polarization achieved during the present experiment.

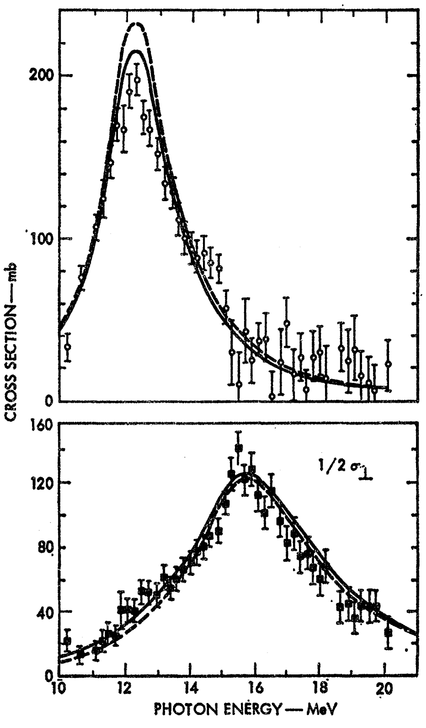

Fig. 16. The intrinsic cross sections for Ho^{165}. The cross section $\sigma_{||}$ is associated with vibrations along the nuclear symmetry axis; $\sigma_\perp$ is that associated with vibrations perpendicular to this axis. The error bars represent statistical errors, and not those due to the uncertainty of f_2. The solid curves are those derived from the elementary collective model; the dashed ones are calculated from the dynamic collective model.

TABLE V. Parameters used for comparing the dynamic collective model with the data. E_R, E_γ, and E_β are the energies of the rotational, γ, and β vibrational degrees of freedom, respectively. E_0 and δ are defined in Eq. (19), and α is the exchange force correction. Reference 11 gives $\Gamma_0=2.1$ MeV, $\alpha=0.16$, and $\delta=1.5$ with this set of parameters. The modifications were made to improve the fit to the present unpolarized data.

E_R (keV)	E_γ (MeV)	E_β (MeV)	E_0 (MeV)	Γ_0 (MeV)	α	δ
10.5	1.0	1.46	12.0	2.3	0.18	2.0

ized and oriented at an angle θ from the photon beam direction. From the data, $A_t=309\pm20$ MeV mb (see Fig. 12), and from the model $A_t=418$ MeV mb, assuming the model is described by the two Lorentz curve fits (Table IV). The ratio is

$$A_t(\text{observed})/A_t(\text{model})=0.74\pm0.05.$$

If the uncertainty of the alignment parameter f_2 is included, the error in this quantity becomes ±0.13. Thus, the observed anisotropy is $(74\pm13)\%$ of what the simple model predicts.

This lower anisotropy is presumably a result of an isotropic component in the giant resonance, resulting either from: (a) an overlapping of the dipole strengths of $\sigma_{||}$ and $\sigma_\perp$ (an equal amount at the same energy would result in an isotropic contribution); (b) a coupling of $\sigma_{||}$ and $\sigma_\perp$ in such a way as to make an isotropic component; or (c) some less energy-dependent mechanism, e.g., the direct reaction processes that Ambler *et al.* suggest.[6] To explain the discrepancy by the last mechanism, about 25% of the total dipole strength (~690 MeV mb) would have to be isotropic. This is considerably larger than one would expect from direct processes, although the intrinsic cross sections (Fig. 16) are consistent with a small isotropic component, varying little with energy over the giant resonance, which might contribute as much as 10% to the integrated cross section.

The following, however, suggests that this isotropic component results from alternative (a) above. Looking at the intrinsic cross sections, there appears to be a second resonance associated with $\sigma_{||}$ at about 14.5 MeV and a change in slope $\sigma_\perp$ at the same energy. There is, consequently, more dipole strength in the region above 14 MeV from $\sigma_{||}$ than a single Lorentz curve would provide, while the same is true for $\sigma_\perp$ in the region below 14 MeV. Such an overlapping of the dipole strengths would cause the observed anisotropy to be low and, depending on the distribution of the dipole strengths, also could explain why the integrated cross section in the higher energy peak of the unpolarized data is larger than the model predicts.

Thus, while this elementary model explains qualitatively the effects of nuclear polarization, it predicts a larger anisotropy in the giant resonance than was observed. The shapes of the intrinsic cross sections suggest that the model does not adequately describe the detailed distribution of the dipole strengths in the giant resonance.

2. *Dynamic Collective Theory*

As was mentioned in the brief review in Sec. I, the dynamic collective theory of Danos and Greiner attributes the giant dipole resonance to the same mechanism as does the more elementary model just discussed. But, by considering the coupling of the giant dipole vibrations to the lower-energy collective phenomena described by the Bohr-Mottelson theory, the energy spectrum associated with the giant resonance becomes considerably richer. Arenhövel *et al.*[11] have compared the predictions of this model with most of the existing measurements of photon absorption and photon scattering cross sections and, in most cases, the agreement is excellent. As is the case in the simple model, the widths of the individual resonances Γ_n cannot be calculated, so these authors assume a smooth variation of Γ_n with energy

$$\Gamma_n=\Gamma_0(E_n/E_0)^\delta, \tag{19}$$

where Γ_0, E_0, and δ are chosen to obtain a reasonable fit to the data. Typically $\Gamma_0=2.3$ MeV, $E_0=12$ MeV, and $\delta=1.5$.

Unfortunately, some of the parameters needed to calculate the dipole strengths for Ho^{165} from this model are not well determined, notably the energy of the γ surface vibrations E_γ. The shape of the giant resonance is strongly affected by the value of E_γ chosen, and Arenhövel *et al.* have taken this as a free parameter in fitting the experimental data available. They list two sets of model parameters for Ho^{165}, one set chosen to fit the unpolarized data of another laboratory,[9] the other to fit an earlier measurement from this laboratory.[10] The two differ primarily in the values chosen for E_γ and β_0, the ground-state deformation. A set of dipole strengths associated with the latter set of parameters are given in Table VI, and with the aid of Eq. (8), cross sections for the polarization achieved in the present experiment have been calculated. In order to improve the fit between these calculated cross sections and the present unpolarized data, the parameters given in Ref. 11 were modified somewhat (see Tables V and VI). The unpolarized cross sections calculated from them are compared with the present unpolarized data in Fig. 17.

The cross sections calculated for the polarized target

TABLE VI. Dipole strengths $|\langle n|Q_1|i\rangle|^2$ calculated for the polarization conditions achieved during the experiment.[a]

ΔK	E_n[b] (MeV)	Γ_n (MeV)	Target unpolarized	Target ∥ photon beam $\sigma_t(0°)$	Target ⊥ photon beam $\sigma_t(90°)$
0	12.25	2.40	0.578	0.371	0.677
	13.81	3.05	0.021	0.014	0.025
±1	15.10	3.64	0.382	0.452	0.350
	16.31	4.25	0.402	0.474	0.368
	16.87	4.55	0.060	0.071	0.055
	18.92	5.72	0.046	0.054	0.042

[a] These dipole strengths represent the major contributions to the dipole cross section. Many small satellites that differ little in energy were grouped together. A complete listing of the dipole strengths for these two sets of parameters were supplied by Dr. H. Arenhövel.

[b] The energy scale of Ref. 11 was multiplied by 1.017 so that the energy calculated for the lower peak of the giant resonance agrees with the present measured value.

are the dashed curves in Fig. 15. These are very similar to the cross sections calculated from the elementary model, as the figure shows. The total anisotropy A_t defined in Eq. (18) is 416 MeV mb for the dynamic collective model, very nearly the same as that obtained from the elementary model.

The intrinsic cross sections calculated from the dynamic collective model (the dashed curves in Fig. 16) are also very similar to those from the elementary model. It is, however, interesting to note that the model does predict a small satellite associated with $\sigma_{\|}$ due to the excitation of one β-vibrational quantum in addition to the giant dipole excitation. It is lower in energy, though (~13.5 MeV), and does not possess as much dipole strength as does the one experimentally observed at 14.5 MeV.

V. SUMMARY AND CONCLUSIONS

Monoenergetic photons obtained from the annihilation in flight of fast positrons were used to measure the photoneutron cross sections of a polarized Ho^{165} target for the cases where the photon beam was parallel and perpendicular to the polarization axis.

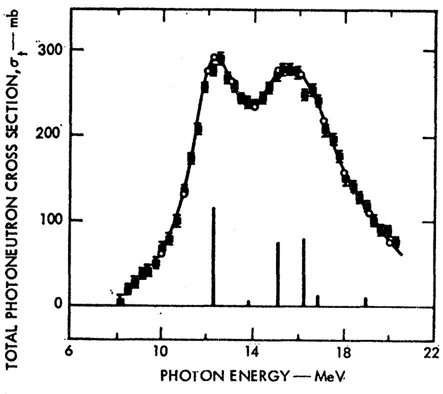

FIG. 17. Fit of the dynamic collective model to the unpolarized Ho^{165} cross sections. The data are those shown in Fig. 9; the smooth curve is calculated from the parameters in Tables V and VI. The vertical bars below the cross-section curve represent the relative dipole strengths.

For each orientation of the target, the total photoneutron cross section was measured. The data for each orientation were compared with measurements of the cross sections for unpolarized Ho^{165} taken at 4.2°K.

The use of a large sample (50 g) of Ho^{165} and the hfs method of polarization yielded measurements having high statistical accuracy, with negligible corrections required for the presence of other materials.

The use of monoenergetic photons yielded cross sections which required no unfolding of photon spectra, and thus, eliminated a major source of uncertainty in the measurements.

The polarization of the Ho^{165} target was confirmed by an independent measurement of the γ-ray anisotropy of γ rays from the disintegration of Ho^{166m}. An alignment parameter $f_2 \cong 0.43$, or 80% of the theoretical maximum, was attained.

The giant resonance cross-section data for the two orientations of the polarized target were analyzed by evaluating the intrinsic cross sections $\sigma_{\|}$ and $\sigma_{\perp}$ from which a figure of merit for the asymmetry was obtained.

The results agree qualitatively with either the elementary or the dynamic collective models in over-all energy dependence of the anisotropy in the giant resonance. However, the magnitude of the anisotropy predicted by both collective models is (25±13)% larger than that observed experimentally. A possible explanation for this discrepancy is provided by the shape of the intrinsic cross sections calculated from the data. These show that the dipole strengths associated with the intrinsic coordinates of the nucleus $\sigma_{\|}$ and $\sigma_{\perp}$ overlap each other to a greater extent than the models predict, thereby reducing the observed anisotropy.

The intrinsic cross sections derived from the data provide some information about the distribution of the dipole strength in the giant resonance, and have several interesting features. The mode associated with the nuclear symmetry axis $\sigma_{||}$ appears to be a doublet, the higher component of which may be a vibrational satellite predicted by the dynamic collective model. The other mode $\sigma_{\perp}$ has a broad base but a sharp peak, suggesting a distribution of dipole strengths somewhat different than that calculated from either of the collective models discussed.

ACKNOWLEDGMENTS

The authors wish to thank Mark Carpenter, Jerry Sawyer, and Dr. J. T. Caldwell for their assistance while the data were being taken, James Nutter and the Linac mechanical technicians for their help with the polarized target, and E. Dante and the Linac operators for their help in performing the experiment. Comments and suggestions about the manuscript received from Dr. H. Arenhövel are also greatly appreciated.

PHYSICAL REVIEW VOLUME 179, NUMBER 4 20 MARCH 1969

Study of the $Zr^{94}(He^3, d)Nb^{95}$ Reaction*

H. OHNUMA† AND J. L. YNTEMA
Argonne National Laboratory, Argonne, Illinois 60439

(Received 25 November 1968)

The $Zr^{94}(He^3, d)Nb^{95}$ reaction was studied with 34-MeV He^3 particles from the Argonne cyclotron. Experimental angular distributions were analyzed on the basis of the distorted-wave Born-approximation theory to determine the l values and spectroscopic factors. The results are compared with the previous data on the (d, He^3) reactions on Mo and Zr isotopes, and the proton configurations of the nuclei in this region are discussed.

I. INTRODUCTION

THE proton structure of nuclei in the region near $N=50$ has been extensively studied, mainly by single-nucleon stripping and pickup reactions.[1-3] The results seem to support the shell-model calculations[4,5] with the assumptions of the Sr^{88} core, in spite of the fact that states with large $p_{3/2}$ and $f_{5/2}$ strength were observed[2,3] at very low excitation energies. It may be interesting to study the (He^3, d) reactions on the nuclei in this region in order to compare the results with those from (d, He^3) reactions. In this paper the results of the $Zr^{94}(He^3, d)Nb^{95}$ reaction are reported.

II. EXPERIMENTAL PROCEDURES AND ANALYSIS

Details of the experiments and analysis were given in the previous paper[3] and will not be repeated here. The experiments were done in the 60-in. scattering chamber[6] with the 34-MeV He^3 beam of the Argonne cyclotron. A (dE/dx)-E telescope consisting of surface-barrier silicon detectors was used for particle detection. Self-supporting metallic zirconium foils, 960 $\mu g/cm^2$ thick and enriched to 95% in Zr^{94}, were used. The angular distributions obtained were compared with distorted-wave Born-approximation (DWBA) calculations performed with the code JULIE[7] and the optical-model parameters listed in Table I. The normalization factor[8] used was 3.84.

III. RESULTS AND DISCUSSION

A typical deuteron spectrum of 20° is shown in Fig. 1. Angular distributions for the low-lying states of Nb^{95} are given in Fig. 2, where the solid and dashed curves show the DWBA calculations. For unresolved states, solid curves represent the sums of two dashed lines. Separation of the angular distributions in the latter cases was found rather difficult and unreliable; since both $l=1$ and $l=4$ angular distributions have their maximum around 19°, the shapes of the summed curves are not sensitive to the relative amplitudes of the two components. Therefore, the assignments and spectroscopic factors for the unresolved states should

---

* Work performed under the auspices of the U.S. Atomic Energy Commission.

† Present address: School of Physics, University of Minnesota, Minneapolis, Minn. 55455.

[1] S. Bjornholm, O. B. Nielson, and R. K. Sheline, Phys. Rev. **115**, 1613 (1959); J. L. Yntema, Phys. Letters **11**, 140 (1964); R. B. Day, A. G. Blair, and D. D. Armstrong, *ibid.* **9**, 327 (1964); C. B. Fulmer and J. B. Ball, Phys. Rev. **140**, B331 (1965).

[2] B. M. Preedom, E. Newman, and J. C. Heibert, Phys. Rev. **166**, 1156 (1968).

[3] H. Ohnuma and J. L. Yntema, Phys. Rev. **176**, 1416 (1968).

[4] I. Talmi and I. Unna, Nucl. Phys. **19**, 225 (1960); N. Auerbach and I. Talmi, *ibid.* **64**, 458 (1965); S. Cohen, R. D. Lawson, M. H. Macfarlane, and M. Soga, Phys. Letters **10**, 195 (1964).

[5] J. Vervier, Nucl. Phys. **75**, 17 (1966).

[6] J. L. Yntema and H. W. Ostrander, Nucl. Instr. Methods **16**, 69 (1962).

[7] R. H. Bassel, R. M. Drisko, and G. R. Satchler, Oak Ridge National Laboratory Report No. ORNL-3240 (unpublished).

[8] R. H. Bassel, Phys. Rev. **149**, 791 (1966).